A single gold metasurface design capable of generating vortex beams with different topological charges

XIAODONG ZHANG[a,b,c,*], DEPENG KONG[a,b], YUAN YUAN[a,b], SEN MEI[a,b], LILI WANG[a,b]
[a]*State Key Laboratory of Transient and Photonics, Xi'an Institute of Optics and Precision Mechanics, Chinese Academy of Sciences, Xi'an 710119, China*
[b]*University of Chinese Academy of Sciences, Beijing 100049, China*
[c]*School of Physics and Electronic Engineering, Zhengzhou University of Light Industry, Zhengzhou 450002, China*

A simple approach is proposed to generate vortex beams using a metasurface composed of 31×31 array of sub-wavelength sized rectangular apertures in a ultrathin gold film. It operates at broadband (800~2000 nm) covering telecom wavelengths, topological charges of resultant vortex beams are from -4 to +4 and weight coefficient of the desired charge exceeds 0.95 under the incidence of circularly polarized light. Simulation results show that this design is logically coincidence. The designed metasurface also has advantage of favorable fabrication tolerance and may be a potential candidate in integrated optical communication system in future.

(Received June 13, 2018; accepted December 10, 2019)

Keywords: Vortex beam, Metasurface, Space-variant polarization

1. Introduction

Orbital angular momentum (OAM) of photon, as proposed by Allen *et al*. [1], is associated with circular polarization has a value of $\pm\hbar$ per photon while an optical vortex beam carries an orbital angular momentum (OAM) of $L\hbar$ per photon. Vortex beam has a helical phase front $\exp(iL\varphi)$, where φ and L are the azimuth angle and topological charge respectively. Generally, vortex beam with OAM is characterized by spiral phase wave fronts in terms of the radiation patterns and hollow magnitudes near its propagation axis. Different OAMs are classified by the topological charge (L) and OAM of vortex beam has unlimited number of eigenmodes (L=1, 2, 3…). Therefore, it offers an additional freedom besides polarization state, amplitude and wavelength for optical communication applications [2, 3]. Due to fascinating properties of OAM, there are many conventional optical elements capable of generating vortex beam, such as spiral phase plate, spatial light modulator, cylindrical lens [4-7] *et al*. But these devices are bulky, and not scalable to sub-wavelength size for integrated optical communication. Compared to conventional optical devices, metasurfaces have advantages of facilitating strong light-matter interaction on a subwavelength scale, eliminating the higher order diffraction of beam, and allowing abrupt changes of beam parameters, controlling the polarization, phase and amplitude of beam in sub-wavelength resolution [8, 9]. Meanwhile, nano-etching fabrication technology has made metasurfaces very promising for integration on a photonic chip [10].

Since Ebbesen *et al*. [11-13] discovered the phenomenon of extraordinary optical transmission through the sub-wavelength sized periodic aperture arrays on metal films for the first time, then Hasman *et al*. [14-17] derived that output light could acquire an additional phase, so-called Pancharatnam-Berry (PB) geometrical phase, by changing the polarization state of it. Due to metallic PB-phase metasurfaces have characteristics of simple principle, easy design, broadband, indispersion *etc.* more and more groups have shifted their interests to this field. As early as 2006, Ruan *et al*. [18] constructed the geometrical size of sub-wavelength aperture applicable to infrared band, then Kang *et al*. [19, 20] designed a metasurface generating vortex beam with topological charge number (L=1) based on PB phase. Later, Zhao *et al*. [21, 22] designed metallic metasurface that generated vortex beam with topological charge from -3 to 3.

In order to develop high efficient vortex-beam-based metasurface photonics devices, we design a metasurface to achieve vortex beam under the incidence of circularly polarized (CP) light. The designed metasurface is composed of spatial-variant, sub-wavelength sized rectangular apertures based on an ultrathin Au film. It operates at wavelengths from 800 nm to 2000 nm, topological charges of resultant beams are from -4 to +4, weight coefficient of the desired charge exceeds 95% and it has advantage of high fabrication tolerance.

2. Structure and theory

The single rectangular aperture unit perforated in an ultrathin gold film is modeled as a size of $l \times w$, a thickness of h and a lattice constant of d, as shown in Fig. 1(a). We investigated the normalized intensity of it at the wavelength from 800 to 2000 nm under the incidence of linearly polarized (LP) light. The numerical simulations were performed based on the finite difference time domain (FDTD) methods. Periodic boundary conditions were applied in the x- and y-directions and perfectly matched layers (PML) conditions were applied in the z-direction. And, refraction index of Au had been considered for more accurate results. Here $T_{\perp}$ denotes the normalized intensity of output light when the input light's polarization direction is perpendicular to aperture direction while $T_{\parallel}$ denotes that when the input light's polarization direction is parallel to aperture direction. Because the mediation between localized waveguide modes and surface plasmon polariton (SPP) modes contributes to transmission and polarization [23-26], as can be seen from Fig. 1(b), $T_{\perp}$ is above 0.2 over a 1200 nm bandwidth (0.8~2.0 μm) basically, and reaches its highest value, 0.79, at 1550 nm, however, $T_{\parallel}$ is less than 0.01 over the whole bandwidth. Thus, we define the extinction ratio (ER) as $10\times\log_{10}(T_{\perp}/T_{\parallel})$ which can exceed 25 dB over the bandwidth. According to simulation results, we can infer that these designed rectangle apertures can be regarded as local spatial-variant linear polarizers with high performance over a whole bandwidth.

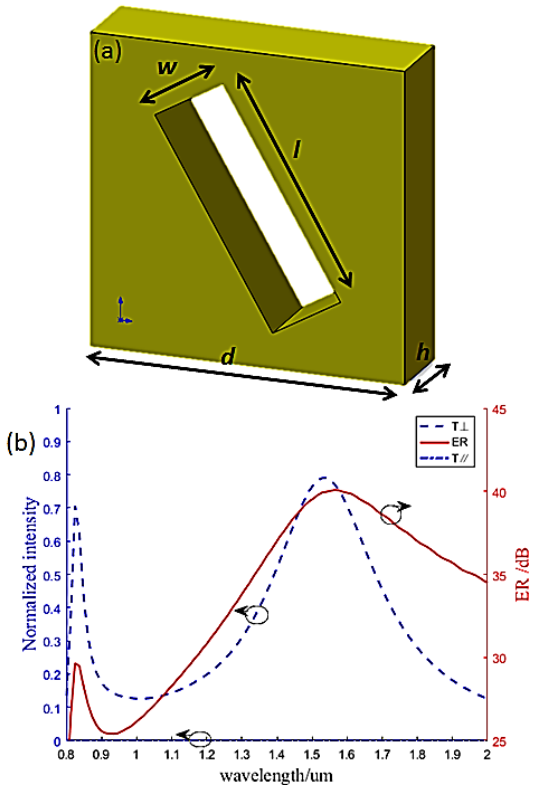

Fig. 1. (a) Dimensions of rectangular aperture: l=630 nm, w=140 nm, h=200 nm, d=700 nm, (b) the normalized intensity ($T_{\perp}$ and $T_{/\!/}$) and the extinction ratio (ER) dependence on input wavelength for the single rectangular aperture unit

In this case, an ultrathin Au film has a size of 21.7×21.7 μm and a thickness of 200 nm. These sub-wavelength sized rectangular apertures perforated in an ultrathin Au film are distributed by 31×31 array and rotated by $\theta(\varphi)$, θ and φ are gradually variant rotation angle and azimuth angle of every rectangular aperture respectively, the relation of them further satisfies $\theta(\varphi)=m\varphi+\alpha_0$, where m and α_0 represent the constructive parameter of metasurface and the initial polarization orientation for $\varphi=0$ respectively ($\alpha_0=0$ in this design), as indicated in Fig. 2(a) and 2(b). The geometric parameters of each rectangular aperture are the same as the single aperture above mentioned, as indicated in Fig. 2(c).

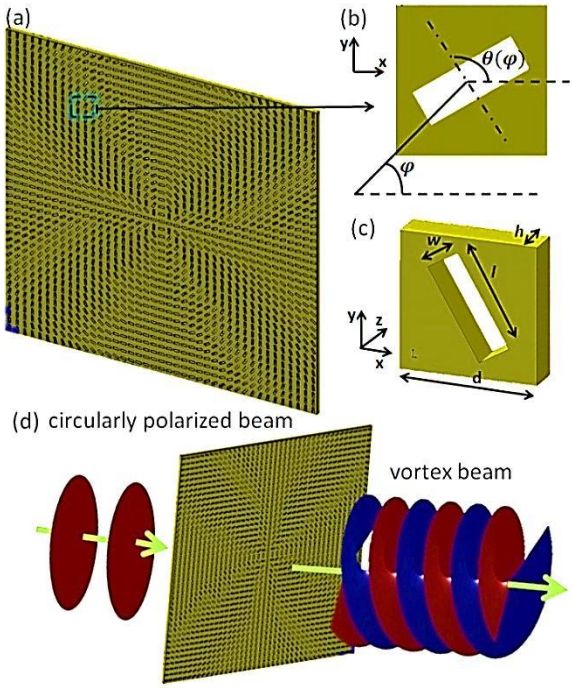

Fig. 2. Schematic structure of the designed metasurface (a) geometric parameters of gold film: 21.7×21.7×0.2 μm, sub-wavelength sized rectangular apertures are perforated in an ultrathin Au film and arranged by 31×31 array distributed uniformly, (b) θ and φ are gradually variant rotation angle and azimuth angle of every rectangular aperture respectively, (c) dimensions of rectangular aperture: l=630 nm, w=140 nm, h=200 nm, d=700 nm, (d) illustration of converting circularly polarized light to vortex beam

Next, we use Jones calculus to mathematically show the evolution of generating vortex beams with different topological charges after CP beam passing though the designed metasurfaces, as shown in Fig. 2(d). For simplicity, we assume an incident plane light as $E_{in}=E_0\begin{pmatrix}1\\ i\sigma\end{pmatrix}$, where, σ=±1 denotes left circularly polarized

(LCP) or right circularly polarized (RCP) light. The Jones matrix for wave plate can be written as, $J=\begin{pmatrix} t_f & 0 \\ 0 & t_s e^{i\delta} \end{pmatrix}$

where t_s and t_f are the transmission coefficients along the optical slow and fast axes and δ is the phase retardation therein. Since sub-wavelength sized rectangular aperture can be regarded as a localized linear polarizer with polarization direction perpendicular to aperture direction [27], then the Jones matrix of that is simplified to $J=\begin{pmatrix} 0 & 0 \\ 0 & 1 \end{pmatrix}$. When pass axis of it makes an angle θ with x axis, the new transmission matrix T for it can be expressed as

$$\begin{aligned} \mathrm{T} &= \mathrm{M}^{-1}(\theta)\times J\times M(\theta) \\ &= \begin{pmatrix} \sin^2\theta(\varphi) & -\sin\theta(\varphi)\cos\theta(\varphi) \\ -\sin\theta(\varphi)\cos\theta(\varphi) & \cos^2\theta(\varphi) \end{pmatrix} \\ &= \begin{pmatrix} \sin^2\varphi & -\sin\varphi\cos\varphi \\ -\sin\varphi\cos\varphi & \cos^2\varphi \end{pmatrix} \end{aligned} \tag{1}$$

where $M=\begin{pmatrix} \cos\theta & \sin\theta \\ -\sin\theta & \cos\theta \end{pmatrix}$ is a two-dimensional rotation matrix and $\theta(\varphi)=m\varphi+\alpha_0$, here α_0=0. Then CP light illuminating the designed metasurface normally, the output light can be written as:

$$\begin{aligned} E_{out} &= T\times E_{in} \\ &= \begin{pmatrix} \sin^2\varphi & -\sin\varphi\cos\varphi \\ -\sin\varphi\cos\varphi & \cos^2\varphi \end{pmatrix} \times E_0 \begin{pmatrix} 1 \\ i\sigma \end{pmatrix} \\ &= \frac{1}{2}E_0 e^{-i2\sigma\varphi}\begin{pmatrix} 1 \\ -i\sigma \end{pmatrix} + \frac{1}{2}E_0\begin{pmatrix} 1 \\ i\sigma \end{pmatrix} \end{aligned} \tag{2}$$

As can be seen from Eq. (2), if the input light is circularly polarized light, the output lights are superposition of a cross-circularly polarized light with an additional phase retardation $\Delta\Phi = -2\sigma\varphi$ and another co-circularly polarized light without an additional phase, and the intensity of them are same. From the literatures [28, 29], We can know that the additional phase retardation $\Delta\Phi$ is not introduced through optical path differences but results from the geometrical phase of space-variant polarization manipulation. In fact, it is a manifestation of the geometrical Pancharatnam–Berry (PB) phase and we can obtain vortex beam with topological charge ($L = -2\sigma m$) by this design based on PB phase. Equation (2) indicates that the sign of topological charge (L) depends on the handedness of input CP light (σ) and the constructive parameter of metasurface (m).

3. Simulations and discussion

In order to verify properties of our designed metasurfaces, simulations were performed based on FDTD method. CP light was incident light and the wavelength was set to 1310 nm. PML conditions were applied in the xyz-direction, refraction index of Au was considered for more accurate results. First, we design four metasurfaces by the constructive parameter (m = 0.5, 1, 1.5, 2 respectively), as indicated in Fig. 3(i). After input light illuminating the four metasurfaces normally, we obtain the output beams. However, it is worth noting that output beams are superposition of two polarized beams (RCP and LCP beam), according to Eq. (2). In order to separate them, we can deal them with Eq. 3,

$$\begin{bmatrix} E_{LCP} \\ E_{RCP} \end{bmatrix} = \frac{1}{\sqrt{2}}\begin{bmatrix} 1 & i \\ 1 & -i \end{bmatrix}\cdot\begin{bmatrix} E_x \\ E_y \end{bmatrix} \tag{3}$$

Equation 3 just work as the quarter wave plate and linear polarized plate in experiment which separates RCP (LCP) beam from resultant beams. Hence, we can obtain one of the two components, and spatial phase and spatial power distributions of them can be shown in Fig. 3.

As can be seen from Fig. 3, when we use RCP light (σ = -1) as input light, Fig. 3(a) shows spatial phase of LCP output beam and Fig. 3(b) shows polarization pattern and spatial power distribution of LCP output beam, here $P(I)_{LCP(RCP)}$ denotes spatial phase (power) of left circularly polarized (right circularly polarized) beam. Yellow circles, the directions of them represent LCP (RCP) component. It is obvious that LCP output beam has features of vortex beam such as: phase pattern jumping from 0 to 2nπ (n=1, 2, 3, 4), the number of arms in the spiral phase equaling the topological charge, a hollow center in the intensity profile at the beam axis and the ring radius of beam increasing with charge number. In addition, the relation of spiral petals of phase distribution and the constructive parameter satisfies $L = -2\sigma m$ (σ = -1, m = 0.5, 1, 1.5, 2 corresponding to L=1, 2, 3, 4). On the contrary, RCP output beam does not have these features, as indicated in Fig. 3(c) and Fig. 3(d). When we use LCP beam (σ=1) as input light, similarly, Fig. 3(g) show spatial phase of RCP output beam and Fig. 3(h) show polarization pattern and spatial power distribution of RCP output beam while Fig. 3(e) and Fig. 3(f) show them of LCP output beam. It is also obvious that RCP beam has features of vortex beam while LCP beam does not. The relation of L and m also satisfies $L = -2\sigma m$ (σ = 1, m = 0.5, 1, 1.5, 2 corresponding to L= -1, -2, -3, -4). Comparing Fig. 3(a) with Fig. 3(g), we can find that the spiral direction of phase is reversed. Such

phenomenon can be easily explained by $L = -2m\sigma$, where the sign of topological charge (L) is determined by the handedness (σ) of CP input light. Above simulation results show good agreement with the prediction of Eq. (2) and indicate that the designed metasurfaces are capable of generating vortex beams with topological charges (±1, ±2, ±3, ±4).

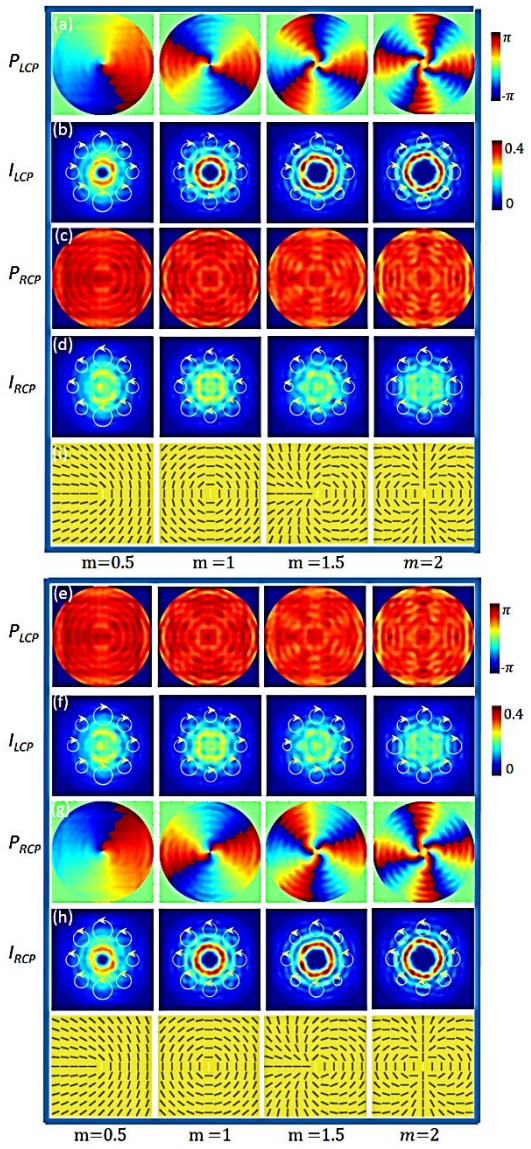

Fig. 3. (a)-(d)Spatial phase distribution, spatial power distribution and polarization pattern of LCP (RCP) output beam under the incidence of RCP light, (e)-(h) under the incidence of LCP light, (i) the designed four metasurfaces (m=0.5, 1, 1.5, 2)

We further conducted a quantitative analysis of vortex beam in terms of the intensity, quantity, ratio and weight. Firstly, we draw the intensities in Fig. 3(b) and Fig. 3(d) along a radial line as a function of the radius. LCP and RCP output results are shown in Fig. 4 respectively. Black (red, blue, green) corresponds to the normalized radial power through the four metasurfaces. Obviously, we can see that the normalized power of LCP beam manifests concentric rings with a hollow center and the radius of the hollow center increases with m while that of RCP beam not, from Fig. 4. Concentric rings with a hollow center owe to the sum of two contributions. One is from the geometrically propagating wave carrying the geometrical phase, the other is from the diverging wave diffracted from the singularity. The interference of the two contributions then leads to the ringing effect [30].

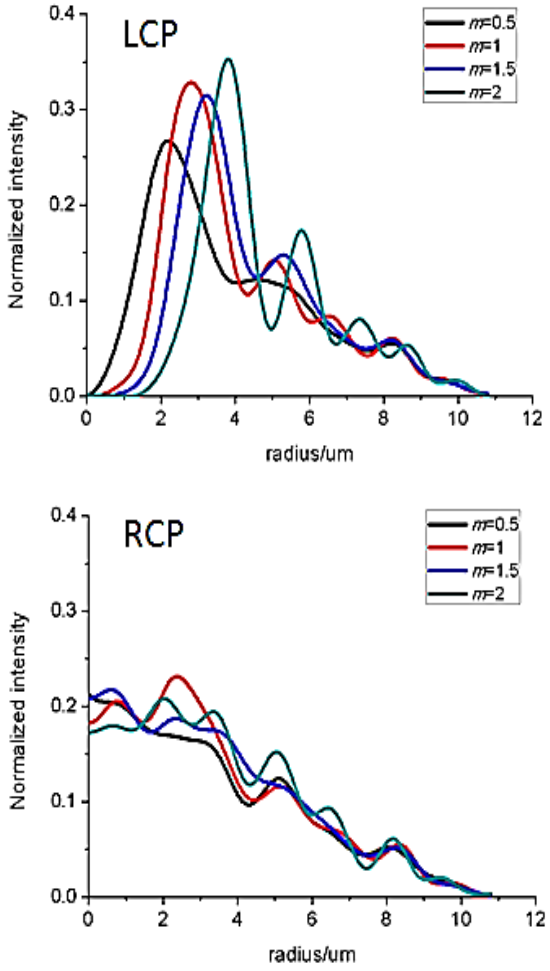

Fig. 4. A radial line power distribution of Fig. 3(b) and Fig. 3(d)

Secondly, we studied on the impact of number of rectangular apertures. We designed the three metasurfaces with the same constructive parameter (m=1), but different array (11×11, 21×21, 31×31 respectively). Here, we still used RCP beam as input light and focused on the wavelength at 1310 nm, spatial phase and spatial power distribution of LCP output beam can be seen from Fig. 5. Obviously, the more number of rectangular apertures is, the better quality of vortex beam is. Meanwhile, vortex beams with more topological charges also can be achieved by adding m. But achieving more topological charges needs further increasing PB phase shift between adjacent apertures which results in discontinuity of spiral phase of

vortex beam and damages the quality of vortex beam greatly within the fixed array, moreover, adding *m* needs increasing the size of array, which makes metasurface too large to compatible for integrated optical communication system.

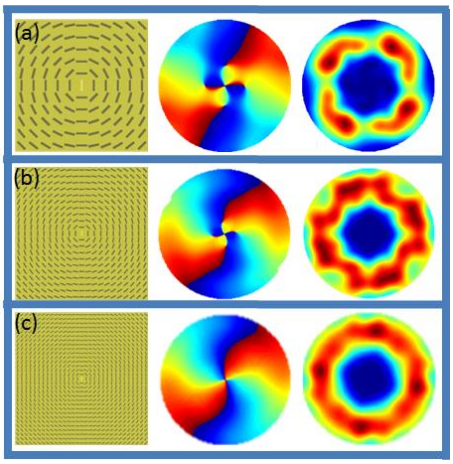

Fig. 5. Spatial phase and spatial power distribution of LCP beam through the three metasurfaces (m=1) (a) 11×11, (b) 21×21, (c) 31×31 array respectively under the incidence of RCP light

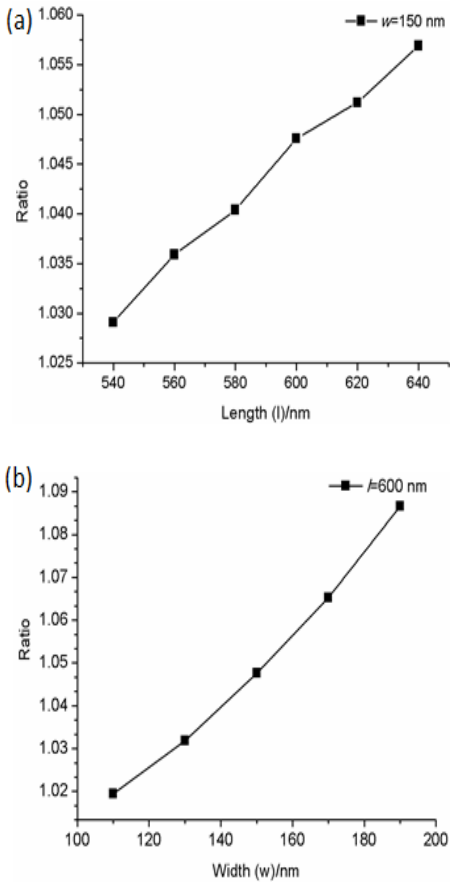

Fig. 6. The dependence of ratio ($\sum I_{LCP}/\sum I_{RCP}$) on (a) length and (b) width of rectangular aperture

Thirdly, we considered the fabrication tolerance by the performance dependence of metasurface on the offset of length and width of aperture. We used RCP light to illuminate the metasurface (*m*=1) at 1310 nm, Fig. 6(a) and 6(b) show ratio which has been defined by $\sum I_{LCP}/\sum I_{RCP}$ as functions of the length (*l*) and width (*w*) of the aperture. $\sum I_{LCP(RCP)}$ denotes that the integrate power of left (right) circularly polarized beam in the monitor. It can be clearly seen that ratio changes slightly around 1.045 with *l* varying from 540 nm to 640 nm (*w*=140 nm) and it also changes slightly around 1.05 with *w* varying from 110 nm to 190 nm (*l*=630 nm). These results imply favorable fabrication tolerance of the designed metasurfaces.

Finally, we computed its projection into the spiral harmonics exp(*inφ*) [31, 32], where *n* is topological charge, *φ* is azimuth angle to determine the weight of the desired topological charge. A output beam with spiral phase can be expressed as

$$E(\rho,\varphi,z)=\frac{1}{\sqrt{2\pi}}\sum_{n=-\infty}^{n=\infty}a_n(\rho,z)\exp(in\varphi) \qquad (4)$$

where $a_n=1/(2\pi)^{1/2}\int_0^{2\pi}E(\rho,\varphi,z)\exp(-in\varphi)d\varphi$, $E(\rho, \varphi, z)$ is the complex electric field, the angular momentum of the beam is given by

$$L_z=(2\varepsilon_0/\omega)\sum_{-\infty}^{\infty}nC_n, \qquad (5)$$

where $C_n=\int_0^r|a_n(\rho,z)|^2\rho d\rho$ and $\sum C_n$=1. Then, C_n is weight coefficient of the nth topological charge. We further define weight spectra of topological charges as $P_n=10\times\log_{10}(C_n/\sum_{q=-\infty}^{\infty}C_q)$. Similarly, we used RCP light to illuminate the four metasurfaces respectively at 1310 nm, and obtained the electric field data. Then converting $E(x, y, z)$ into $E(\rho, \varphi, z)$ in polar coordinate, we calculate the weight coefficient of nine topological charges of output LCP (RCP) beam, as shown in Fig. 7(a) and 7(b). Nine bars (gray bar ~ yellow bar) in Legend represent the weight of topological charge (from -4 to +4) respectively. It is obvious that LCP beam turns into vortex beam with different topological charges while RCP beam not, moreover, the weight spectra of desired topological charge is larger than 0.95 that further validates our designs.

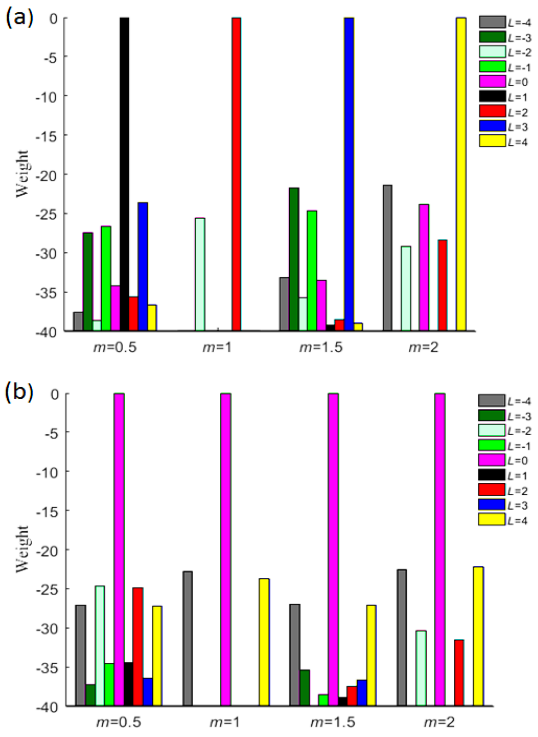

Fig. 7. Under the incidence of RCP light, (a) weight spectra of LCP beam and (b) RCP beam corresponding to the four metasurfaces at 1310 nm

Though we focus on the wavelength at 1310 nm, our designed metasurface is also suitable for other wavelengths, such as 850 nm, 1550 nm etc. It should be noted that this study has examined only the metallic metasurface. Due to nonradiative Ohmic losses in metals etc., the transmission efficiency of the metallic metasurface is less than that of dielectric metasurfaces [33-35]. However our designed metasurface has characteristics of broadband and easy fabrication. Moreover, the transmission efficiency of the design may be improved if the parameters of rectangular apertures are further optimized.

4. Conclusions

In conclusion, we propose a simple approach to generate vortex beam with different topological charges (±1, ±2, ±3, ±4) based on the designed ultrathin Au metasurface. The designed metasurface has characteristics of multi topological charges, high weight coefficient (>0.95), broadband including telecom wavelengths and favorable fabrication tolerance. Simulation results have demonstrated theoretical derivation and validated our designs. With future improvement, we may improve the transmission efficiency by optimizing the geometrical parameters. Our method may provide a potential for integrated optical communication system.

Acknowledgment

This work was supported by the Natural Science Foundation of China (NSFC) [grant numbers 11474351, 61275106, 11504416].

References

[1] L. Allen, R. J. C. Spreeuw, J. P. Woerdman, Physical Review A, **45**(11), 6 (1992).
[2] P. K. P. Gregg, S. Ramachandran1, Optical Fiber Technology **2**(3), 267 (2015).
[3] Q. Zhan, Optics Letters **31**(7), 867 (2006).
[4] W. Y. Huang, J. L. Li, H. Z. Wang, J. P. Wang, S. S. Gao, Electromagnetics **36**(2), 102 (2016).
[5] M. Stalder, M. Schadt, Optics Letters **21**(23), 1948 (1996).
[6] Wei Ji, Chun-Hong Lee, Peng Chen, Wei Hu, Yang Ming, Lijian Zhang, Scientific Reports **6**, 25528 (2016).
[7] M. J. Padgett, L. Allen, Journal of Optics B Quantum & Semiclassical Optics **4**(2), S17 (2002).
[8] S. Yu, L. Li, G. Shi, C. Zhu, X. Zhou, Y. Shi, Applied Physics Letters **108**(12), 121903 (2016).
[9] N. Yu, F. Capasso, Nature Materials **13**(2), 139 (2014).
[10] F. Monticone, A. Alù, Chinese Physics B **23**(4), 64 (2014).
[11] T. W. Ebbesen, H. J. Lezec, H. F. Ghaemi, T. Thio, P. A. Wolff, Nature **391**(6668), 667 (1998).
[12] K. J. Klein Koerkamp, S. Enoch, F. B. Segerink, Physical Review Letters **92**(18),183901 (2004).
[13] L. Martínmoreno, F. J. Garcíavidal, H. J. Lezec, K. M. Pellerin, T. Thio, J. B. Pendry, T. W. Ebbesen, Physical Review Letters **86**(6), 1114 (2001).
[14] G. Biener, A. Niv, V. Kleiner, E. Hasman, Optics Letters **27**(21), 1875 (2002).
[15] E. Hasman, Z. E. Bomzon, A. Niv, G. Biener, V. Kleiner, Optics Communications **209**(1–3), 45 (2002).
[16] Z. Bomzon, G. Biener, V. Kleiner, E. Hasman, Optics Letters **27**(13), 1141(2002).
[17] A. Niv, G. Biener, V. Kleiner, E. Hasman, Optics Express **14**(10), 4208 (2006).
[18] Z. Ruan, M. Qiu, Physical Review Letters **96**(23), 233901 (2006).
[19] M. Kang, J. Chen, B. Gu, Y. Li, L. T. Vuong, H. T. Wang, Physical Review A **85**(3), 8207 (2012).
[20] M. Kang, J. Chen, X. L. Wang, H. T. Wang, Journal of the Optical Society of America B **29**(4), 572 (2012).
[21] Z. Zhao, J. Wang, S. Li, A. E. Willner, Optics Letters **38**(6), 932 (2013).
[22] Z. Zhao, Y. Ren, G. Xie, Y. Yan, Mlillimeter-wave Communications **34**(5), 1392 (2015).
[23] A. Degiron, T. W. Ebbesen, Journal of Optics A: Pure & Applied Optics **7**(2), 5648 (2005).
[24] A. Mary, S. G. Rodrigo, L. Martínmoreno, F. J.

Garcíavidal, Physical Review B Condensed Matter **76**(76), 195414 (2007).
[25] E. Altewischer, M. P. V. Exter, J. P. Woerdman, Journal of the Optical Society of America B **20**(9), 1927 (2002).
[26] F. Miyamaru, T. Kondo, T. Nagashima, M. Tani, Applied Optics **43**(6), 1412 (2004).
[27] A. Degiron, H. J. Lezec, N. Yamamoto, T. W. Ebbesen, Mineralogical Magazine **239**(1–3), 61 (2004).
[28] L. Marrucci, C. Manzo, D. Paparo, Physical Review Letters **96**(16), (2006).
[29] F. Cardano, E. Karimi, S. Slussarenko, L. Marrucci, L. C. De, E. Santamato, Applied Optics **51**(10), C1 (2012).
[30] W. Shu, Y. Liu, Y. Ke, X. Ling, Z. Liu, B. Huang, H. Luo, X. Yin, Optics Express **24**(18), 21177 (2016).
[31] L. Torner, J. Torres, S. Carrasco, Optics Express **13**(3), 873 (2005).
[32] N. Yu, P. Genevet, F. Aieta, M. A. Kats, R. Blanchard, G. Aoust, J. P. Tetienne, Z. Gaburro, F. Capasso, IEEE Journal of Selected Topics in Quantum Electronics **19**(3), 4700423 (2013).
[33] S. Jahani, Z. Jacob, Nature Nanotechnology **11**(1), 23 (2016).
[34] A. Arbabi, Y. Horie, M. Bagheri, A. Faraon, Nature Nanotechnology **10**(11), 937 (2015).
[35] R. C. Devlin, A. Ambrosio, D. Wintz, S. L. Oscurato, A. Y. Zhu, M. Khorasaninejad, J. Oh, P. Maddalena, F. Capasso, Optics Express **25**(1), 377 (2017).

*Corresponding author: zhangxiaodong@opt.cn